CHAPTER IV
RESULTS AND DISCUSSION

4.1 Characterization

4.1.1 Polyaniline

4.1.1.1 Elemental analysis (EA)

EA was used to determine the amount of elements: carbon (C), hydrogen (H) and nitrogen (N) for molecular structure of polyaniline, emeraldine base form, as well as the amount of proton in acid doping process. The molecular compositions of the synthesized polyaniline were calculated as shown in Appendix A. The values of C:H:N determined from emeraldine base from 3 synthesis batches were consistent with the structure of emeraldine base form: $(C_6H_{4.5}N_1)_4$. The amounts of protonated proton were converted to the % doping level as shown in Appendix B. The correlation between the % doping levels and the doping ratios is shown in Figure 4.1.

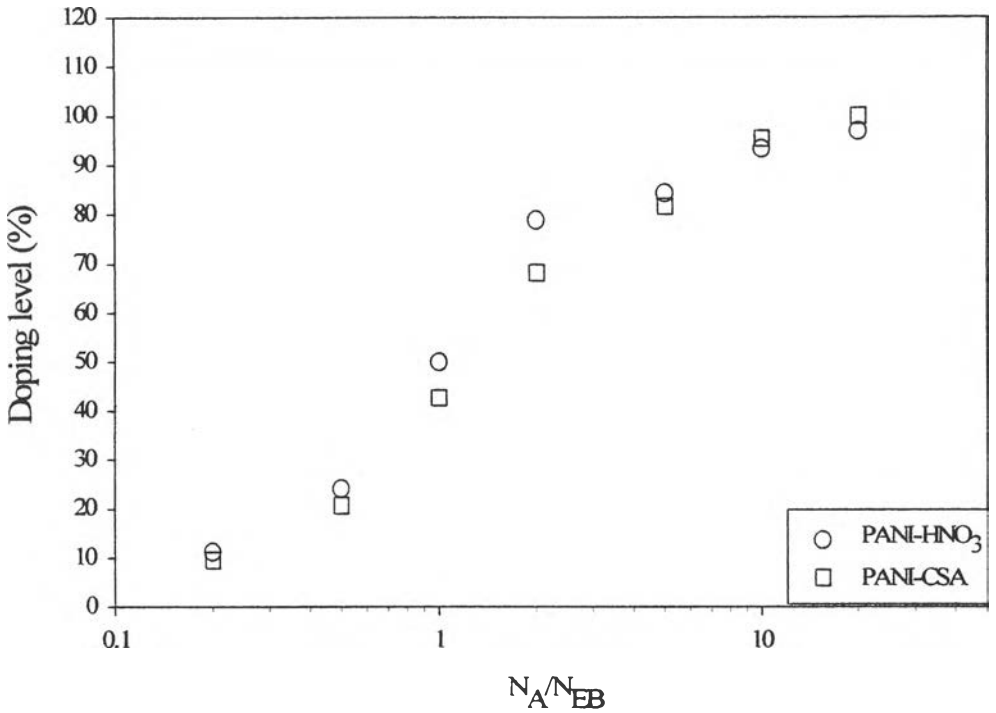

Figure 4.1 Relation between the doping level and doping ratio of PANI-CSA and PANI-HNO_3.

Figure 4.1 shows that the % doping level increases sharply with increasing doping ratio when the doping ratio is less than 5. This was due to the protonation stage from the acid doping process; a greater amount of acid in the solution produced a greater acid protonation on a polyaniline chain. As acid concentration was increased beyond N_A/N_{EB} ~ 10, the % doping level increased slightly and finally reached a plateau. This was because the acid had a lesser chance to be incorporated with the imine nitrogen. This occurred at doping ratios greater than 5.

4.1.1.2 FT-IR spectroscopy

The FT-IR spectra of undoped, PANI-CSA and PANI-HNO_3 were analyzed and the peak locations and interpretations were identified and data were tabulated in Appendix C and Table C.1. In Figure 4.2, characteristic peaks of emeraldine base and doped polyaniline were found at 1493 and 1584 cm^{-1} (Zeng and Ko, 1998); they represent the C=C stretching vibrations of benzenoid segment and –

N= of the quinoid segment. The PANI-CSA and PANI-HNO_3 show additional absorbance peaks: at 1732 and 1035 cm^{-1} due to the stretching of the C=O group and the sulfonic acid salt group for CSA; and at 1530 and 1330 cm^{-1} due to the N-O asymmetric stretching and the vibrational mode of NO_3^- for the PANI-HNO_3 (Kang *et al.*, 1998).

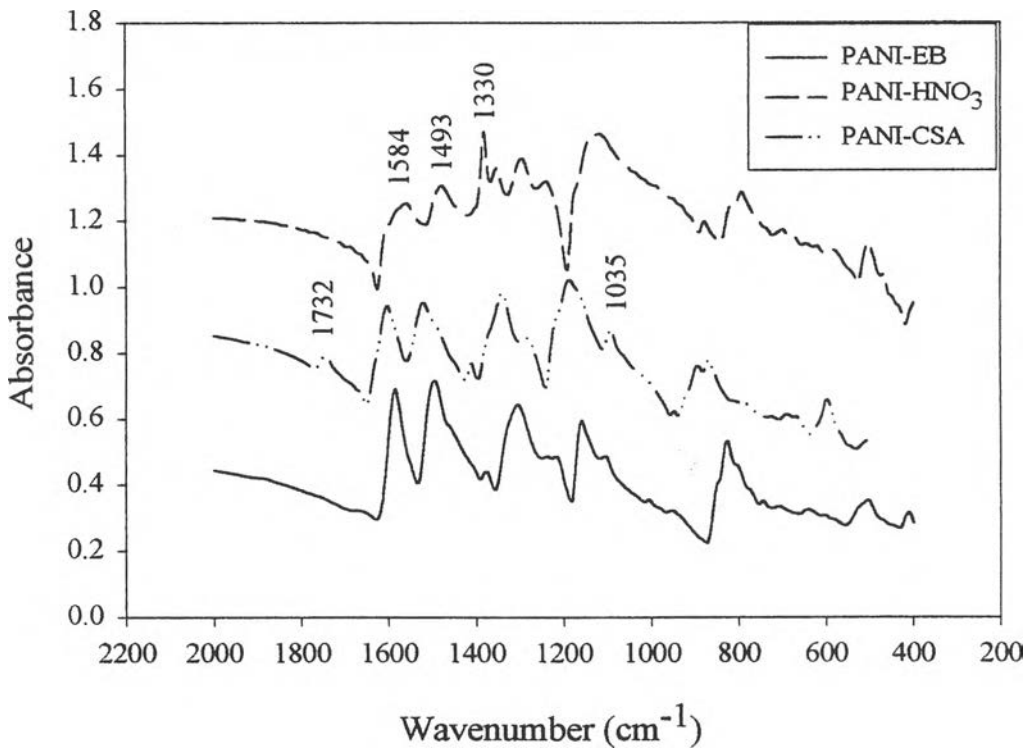

Figure 4.2 FT-IR spectra of undoped, PANI-CSA and PANI-HNO_3.

Upon doping, the intensity and the peak width at 1584 cm^{-1} due to the –N= stretching was decreased but the intensity and the peak width at 1493 cm^{-1} due to the C=C of aromatic stretching remained constant. The % doping levels could be and was calculated from the ratio of the peaks at 1480 and 1584 cm^{-1} to indicate the protonation state of emeraldine salt as shown in Appendix D.

4.1.1.3 EDX

The values of % mole from EDX were used to determine the % doping level of doped polyaniline as calculated and shown in Appendix E. The correlation between the % doping level and the doping ratio from the three methods, which are EA, FT-IR and EDX techniques, are shown in Figure 4.3 and Figure 4.4 for PANI-CSA and PANI-HNO_3, respectively.

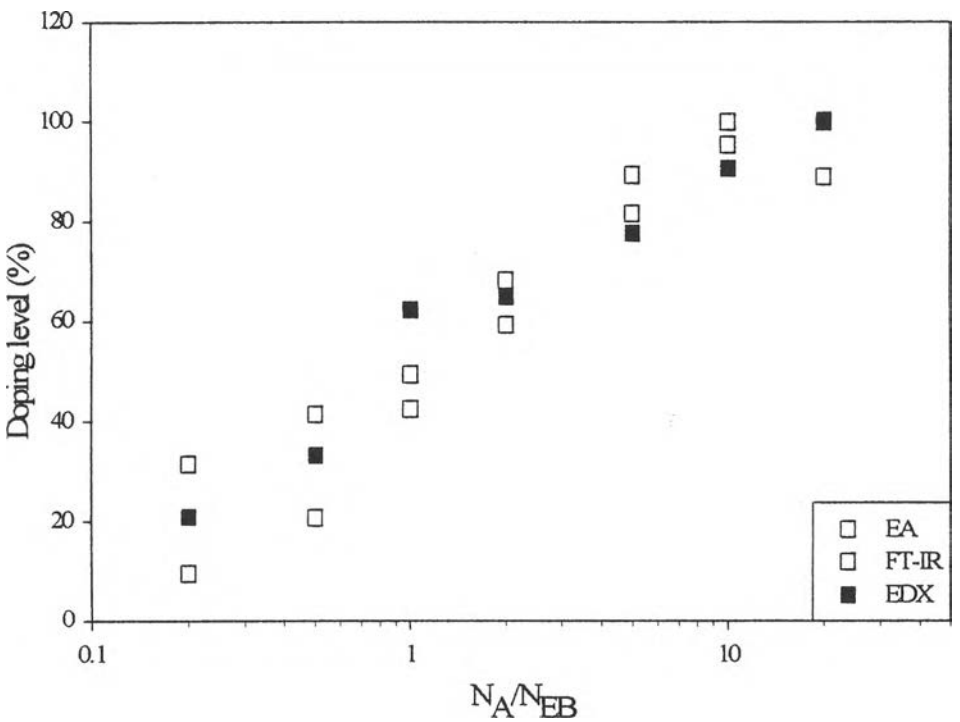

Figure 4.3 Doping level (%) vs. doping ratio of PANI-CSA.

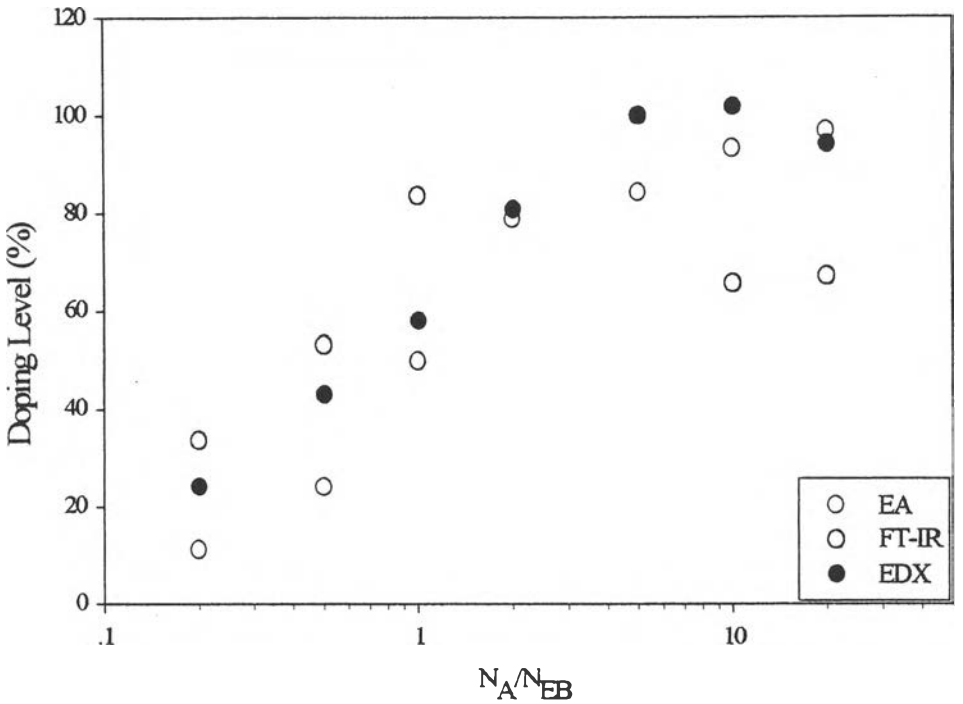

Figure 4.4 Doping level (%) vs. doping ratio of PANI-HNO_3.

From Figure 4.3, the values of % doping level from the three methods are all comparable for PANI-CSA. Only a small difference in each data point was found in each testing method. In Figure 4.4, the value of % doping level calculated from FT-IR method, deviate from those of the other two methods. This was because of the overlapping of the N-O asymmetric stretching at 1530 cm^{-1} with –N= of the quinoid segment at 1584 cm^{-1} (Zeng and Ko, 1998). This overlapping was the major factor causing the data from FT-IR result to deviate from the EA and EDX results. The EDX method is a surface analysis whereas the EA method is a bulk analysis, the latter is considered to be a more accurate one. So the calculated data of the % doping level from the elemental analysis are the most reliable and are used throughout in the remaining of the thesis work.

4.1.1.4 UV-visible spectroscopy

The UV-Visible spectrum of emeraldine base shows two-classical absorption peaks as shown in Figure 4.5. The first one is at 324 nm, which indicates the π–π^* transition electrons of the benzene ring delocalized onto nitrogen atoms of the amine in the benzenoid segments. The second one is at 630 nm, which indicates the excitation from the highest occupied molecular orbital (HOMO π_b) of the benzenoid ring to the lowest unoccupied molecular orbital (LUMO π_q) of the localized quinoid segment (Huang *et al.,* 1993). For a doped polyaniline, it could be seen that the two absorption peaks belonging to the emeraldine base structure disappeared at N_A/N_{EB} greater than 10 and 5 for PANI-CSA and PANI-HNO_3, respectively (Appendix F). For concentrations of acids lower than the quoted values, the acid amounts were not sufficient to convert the emeraldine base to the emeraldine salt in NMP solvent. At the doping ratio greater than the quoted values, there appeared absorption peaks at 430 and 820 nm, representing the bipolaron state and the polaron state, respectively (Zeng *et al.*, 1992).

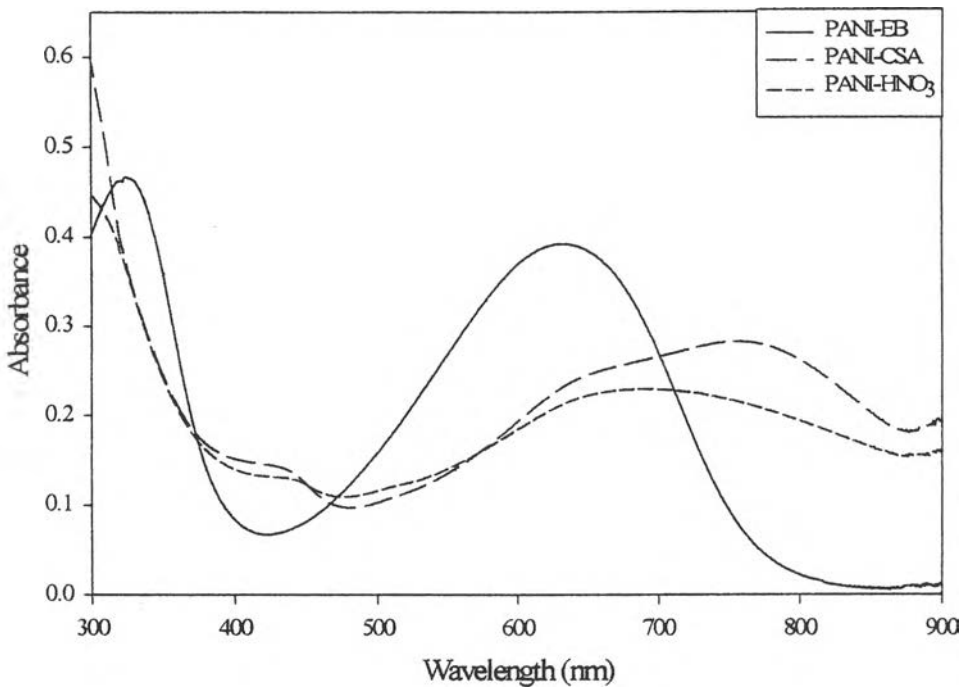

Figure 4.5 UV-visible spectra of undoped, PANI-CSA and PANI-HNO_3.

4.1.1.5 Thermogravimetric analysis (TGA)

The TGA thermogram of emeraldine base in Figure 4.6 shows two-step weight losses at 50-110 and 500-550 °C, due to loss of water and polymer chain degradation, repsectively (Palaniappan and Narayana, 1994). For PANI-HNO_3, three-step weight losses were observed at 50-110, 180-220 and 500-550 °C, due to the loss of water, the loss of dopant and the polymer chain degradation, respectively (Cao *et. al*, 1992). The same weight losses were obtained for PANI-CSA except for the second step; CSA molecules generally degrade at 220-350 °C. The % weight losses of all steps are shown in Appendix G, Tables G.1 and G.2 for PANI-CSA and PANI-HNO_3, respectively. The result of first step % weight loss was used to determine the amount of water content in which the electrical conductivity usually depends on. Swarngwong, J. (2001) concluded that as the amount of moisture content increased, the conductivity increased correspondingly. Throughout this thesis, the amount of % moisture content was controlled and found

to be 5-6.5 % and 7-9 % for PANI-CSA and PANI-HNO_3, respectively. The second step % weight loss, which was due to the loss of dopant, increased with increasing doping ratio for both acids. This result can be used to confirm the data and results of the elemental analysis; the % doping level increased with increasing acid mole ratio due to a greater protonation of acid to polyaniline chain.

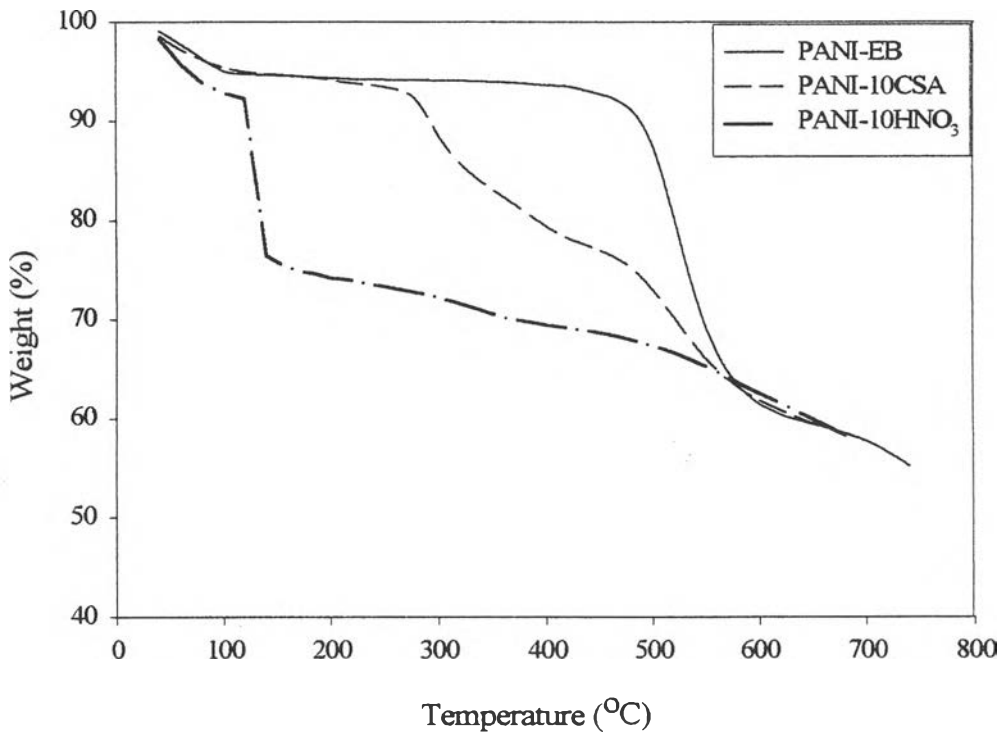

Figure 4.6 TGA thermogram of undoped, PANI-CSA and PANI-HNO_3.

4.1.1.6 X-Ray diffraction (XRD)

The XRD patterns of undoped, PANI-CSA and PANI-HNO_3 are shown in Figure 4.7. The XRD diffraction pattern of emeraldine base was found to be of a typical amorphous polymer. For doped polyanilines, the order and degree of crystallinity at 2θ = 9.5, 14.5, 20.6 and 25.5 represent the Miller indices of (001), (010), (100) and (110), respectively (Winokur *et al.*, 1998). These peaks were used

to determine the degrees of crystallinity of PANI-CSA and PANI-HNO_3 at various doping ratios as shown in Appendix I.

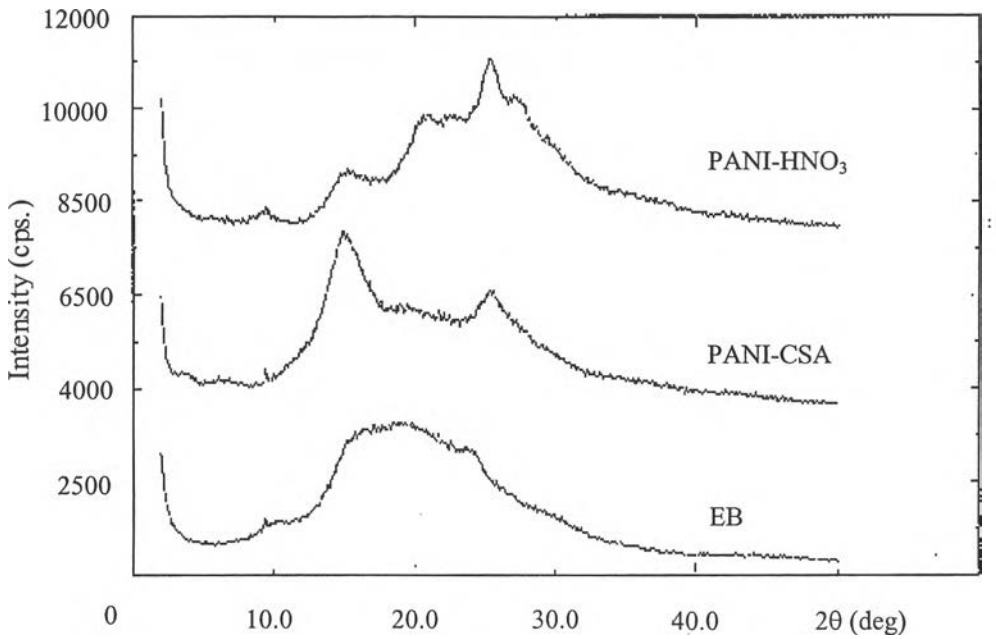

Figure 4.7 XRD patterns of undoped, PANI-CSA and PANI-HNO_3.

From the calculated data of the % crystallinity in Appendix I, it was found that the % crystallinity increased with increasing % doping level. This was due to the interaction between the chains as can be explained by the model proposed by Keattibutr, P. (2000). At a low doping ratio, a partially crystalline structure existed along with a greater distance between polymer chains. On the other hand, at a higher doping ratio a more crystalline structure was found due to the chain expansion, which may have induced a shorter distance between polymer chains.

4.1.1.7 Scanning electron microscope

The SEM micrographs of undoped, PANI-CSA and PANI-HNO_3 are shown in Appendix H and Table H.1. They show a globular morphology. For the PANI-CSA and PANI-HNO_3 and at doping levels higher than 10, we found

fibrillar and plate-like morphology in certain domains. This was due to the higher chain expansion higher % crystallinity at higher doping ratios, as discussed in part 4.1.1.6.

4.1.2 Polyimide

4.1.2.1 Elemental analysis (EA)

EA was used to determine the amounts of elements: carbon (C), hydrogen (H), nitrogen (N) and oxygen (O) for molecular structure of polyimide. The molecular compositions of synthesized polyanilines were calculated as shown in Appendix A. The values of C:H:O:N determined from polyimides synthesized from three batches are consistent with the values of the theoretical structure: $(C_{11}H_5O_{2.5}N_1)_2$.

4.1.2.2 FT-IR spectroscopy

The FT-IR spectra of polyimide were measured, analyzed and the peak locations were identified along with interpretations as tabulated in Appendix C, Table C.2. The FT-IR spectra of PAA and PI are shown in Figure 4.8. After imidisation, the peaks of the –NH stretching and the –OH stretching at 3300 and 3000 cm^{-1} (Asawakanjana, 1997) disappeared. Also, the intensity of the peak at 1780 cm^{-1} due to the C=O symmetric stretching increased. This was due to the transformation from the C=O asymmetric structure of PAA to the C=O symmetric structure of PI (Han *et al.*, 1998).

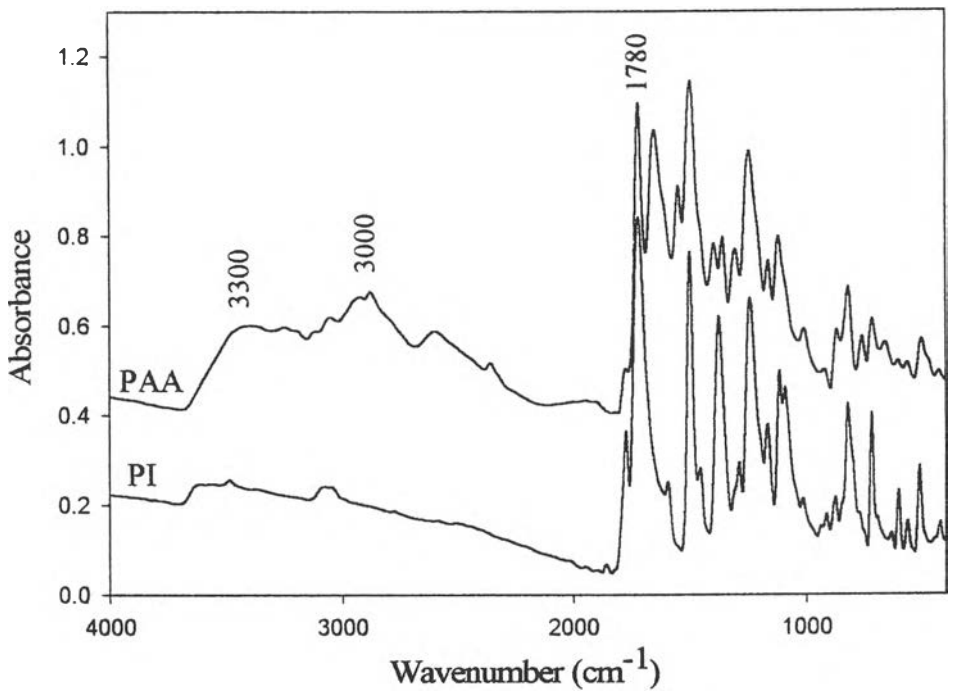

Figure 4.8 FT-IR spectra of PAA and PI.

4.1.2.3 Thermogravimetric analysis (TGA)

The TGA thermogram of poly(amic acid) and polyimide shows two-step weight losses at 160-210 and 550-600 °C, due to solvent molecules and polymer chain degradation (Han *et al.*, 1998) as shown in Figure 4.9. The % weight losses of both steps are shown in Appendix G.

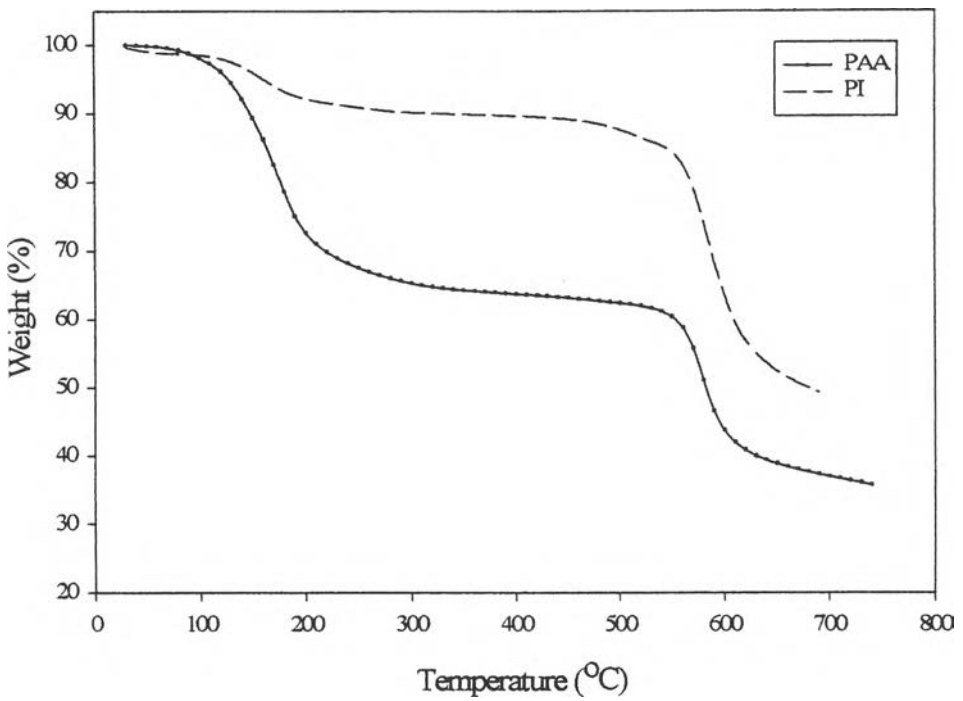

Figure 4.9 TGA thermogram of PAA and PI.

From Figure 4.9, it can be seen that the thermal stability of PI was greatly enhanced after imidisation process as evident from the % weight loss of the first step and this was a result of the more % residue of PI relative to PAA. But the degradation temperature of both PAA and PI were found not to be significantly different.

4.1.2.4 Scanning electron microscope (SEM)

The SEM micrograph of polyimide is shown in Appendix H. It shows a globular morphology structure. Because PI is of the PMDA-ODA type; it is of a semirigid structure whose interchain interaction is moderately strong in forces (Asawakanjana, 1997).

4.1.3 Polyaniline/Polyimide Composites

4.1.3.1 Scanning electron microscope (SEM)

The SEM micrograph of both PANI-CSA/PI and PANI-HNO_3/PI are shown in Appendix H. The composites at various %wt of polyimide show a good dispersion of polyimide in the polyaniline matrix. The separation of both components indicates that the composites were likely to be immiscible blends.

4.1.3.2 Thermogravimetric analysis (TGA)

The TGA thermograms of PANI-CSA/PI and PANI-HNO_3/PI are shown in Figures 4.10 and 4.11, respectively.

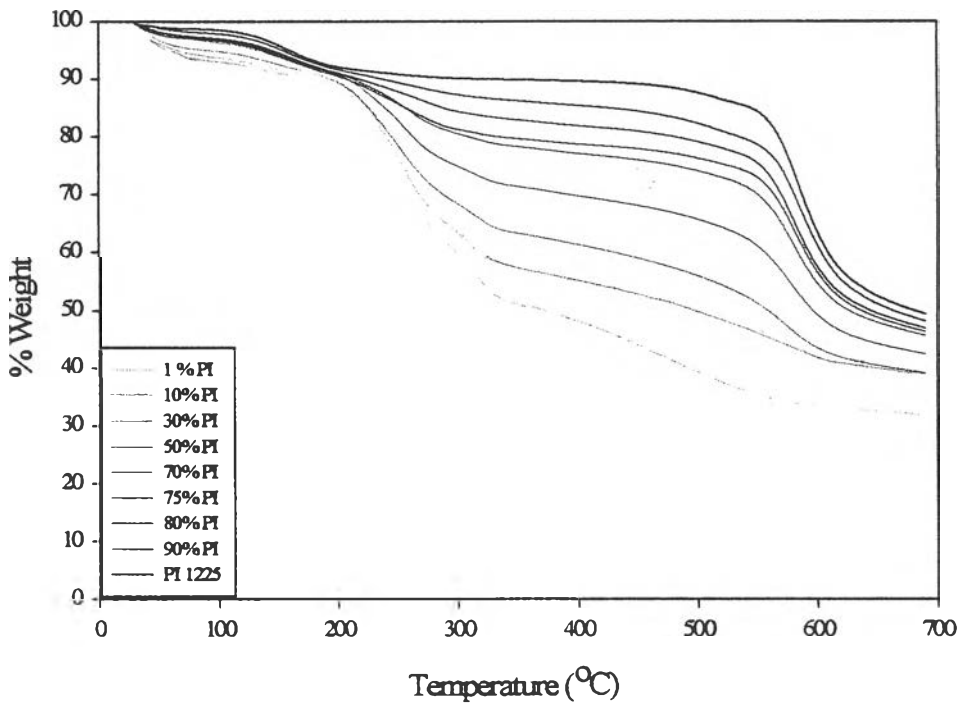

Figure 4.10 TGA thermogram of PANI-CSA/PI at various PI (%wt) in the blend.

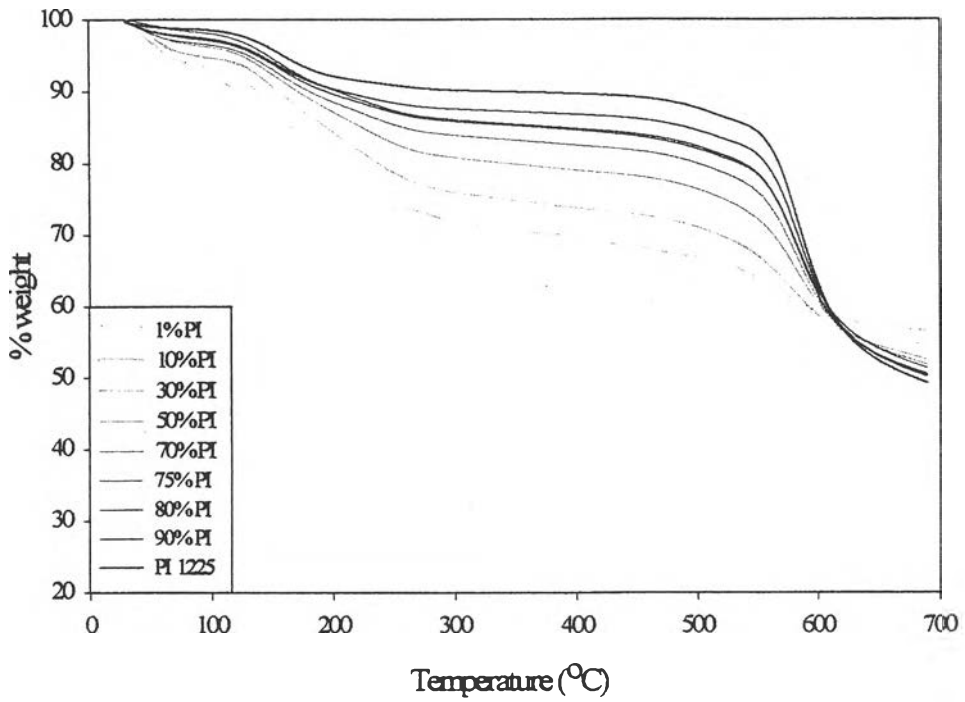

Figure 4.11 TGA thermogram of PANI-HNO_3 blend with polyimide at various PI (%wt) in the blend.

From Figures 4.10 and 4.11, the % weight loss decreases with increasing % of polyimide in the blend. The value of % residue also increased with the % polyimide in the blend for PANI. For PANI-HNO_3, the % residue decreased with increasing % polyimide in the blend. This was due t o the % residue of PANI-HNO_3 was higher than that of polyimide.

4.2 Electrical Conductivity Property

4.2.1 Effect of Acid Dopant Type and Concentration

The specific conductivity values of PANI-CSA and PANI-HNO_3 at various doping ratios of N_A/N_{EB} = 0.2, 0.5, 1.0, 2.0, 5.0, 10.0 and 20.0, at a controlled temperature between 25 ± 2 °C, a relative humidity in air of 48-52 % and at the atmospheric pressure 1 atm, were measured in order to study the effect of acid dopant type and concentration on conductivity. The effects of acid dopant types and concentration on the electrical conductivity of PANI-CSA and PANI-HNO_3 are shown in Figure 4.12.

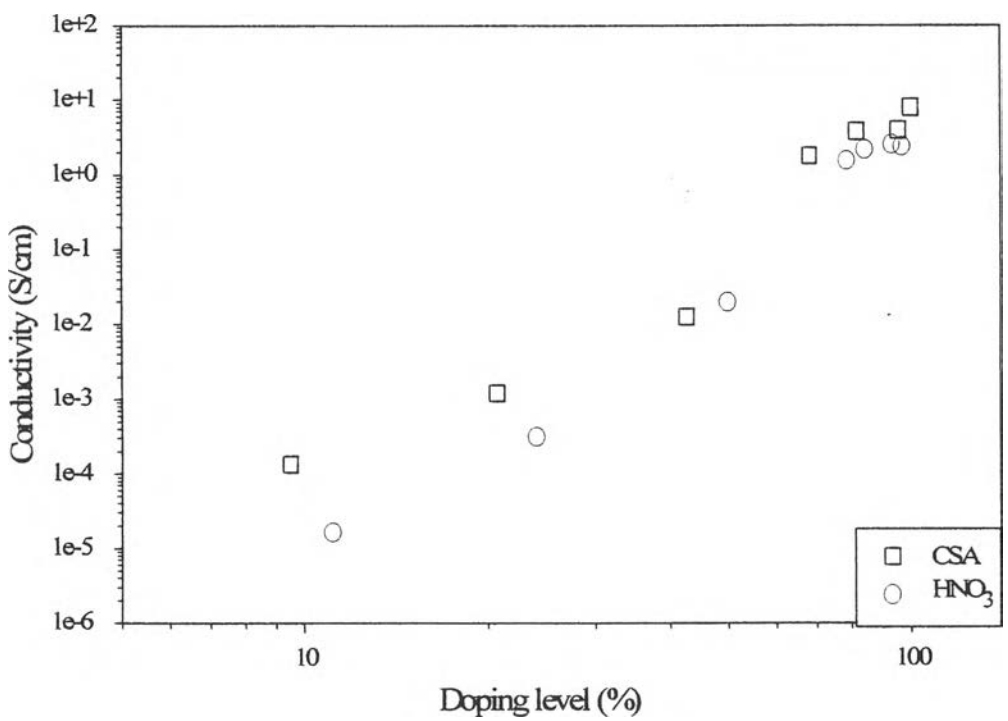

Figure 4.12 Conductivity vs. doping level (%) of PANI-CSA and PANI-HNO_3 (N_A/N_{EB} = 0.2, 0.5, 1.0, 2.0, 5.0, 10.0 and 20.0).

From Figure 4.12, the specific conductivity increases with increasing % doping level for both PANI-CSA and PANI-HNO_3 within the range of the % doping level between 0-70. This was a direct result of a greater degree of protonation of polyaniline, resulting in a greater number of charge carriers and leading to a higher conductivity. Beyond this regime (% doping level > 70%), the specific conductivity reached a plateau of the same order of magnitude. This was considered to be the saturated level of doping, as the proton could not protonate at imine nitrogen any more on polyaniline chains. The saturated or maximum electrical conductivity values attained were at 5.61 and 2.38 S/cm for PANI-CSA and PANI-HNO_3, respectively.

In term of acid dopant type, CSA induced a higher conductivity than PANI-HNO_3 at any values of % doping level. At values of % doping level lower than 30, PANI-CSA had a significantly higher specific conductivity by one order of magnitude. But at values of the % doping level greater than 30, there was no significant difference in the specific conductivity values of both PANI-CSA and PANI-HNO_3. This was because the acid dissociation constant of CSA (-10.43) was lower than that of HNO_3 (1.4), CSA could protonate polyaniline chains easier than HNO_3 because it could dissociate more easily in an aqueous media (Allcock *et. al*, 1990). Moreover, the anionic strength of emeraldine salt of PANI-CSA was higher than that of PANI-HNO_3; a greater positive charge density of imine nitrogen through the structure of emeraldine salt structure was expected for PANI-CSA at low % doping level (< 30). At a higher value of % doping level (>30), the specific conductivity for PANI-CSA was not significantly higher than PANI-HNO_3. This was because the acid concentrations for PANI-CSA and PANI-HNO_3 were sufficiently high to be able to overcome the acid dissociation constant effect. In this % doping level, the anionic strengths of both PANI-CSA and PANI-HNO_3 were comparable leading to no significant difference in the specific conductivity.

Consider the equation: $\sigma = ne\mu$, whereas n is the number of charge carrier (#/volume) and μ is the carrier mobility (m^2/Volt-sec), it is known that the specific conductivity is linearly proportional to the number of charge carrier if the value of carrier mobility is constant. From Figure 4.12, the nonlinearity between specific

conductivity and the number of charge carrier can be seen. This implies that the carrier mobility is not constant, but it is the function of % doping level as can be explained in terms of the effect of % crystallinity in part 4.2.2.

4.2.2 Effect of the % Crystallinity

The specific conductivity values of PANI-CSA and PANI-HNO_3 at various doping ratios of N_A/N_{EB} = 0.2, 0.5, 1.0, 2.0, 5.0, 10.0 and 20.0, at a controlled temperature between 25 ± 2 °C, a relative humidity in air between 48-52 % and at the atmospheric pressure 1 atm were measured in order to study the effect of % crystallinity on the charge carrier mobility. The correlation between the ratio of σ/% doping level and the % crystallinity, of PANI-CSA and PANI-HNO_3, is shown in Figure 4.13.

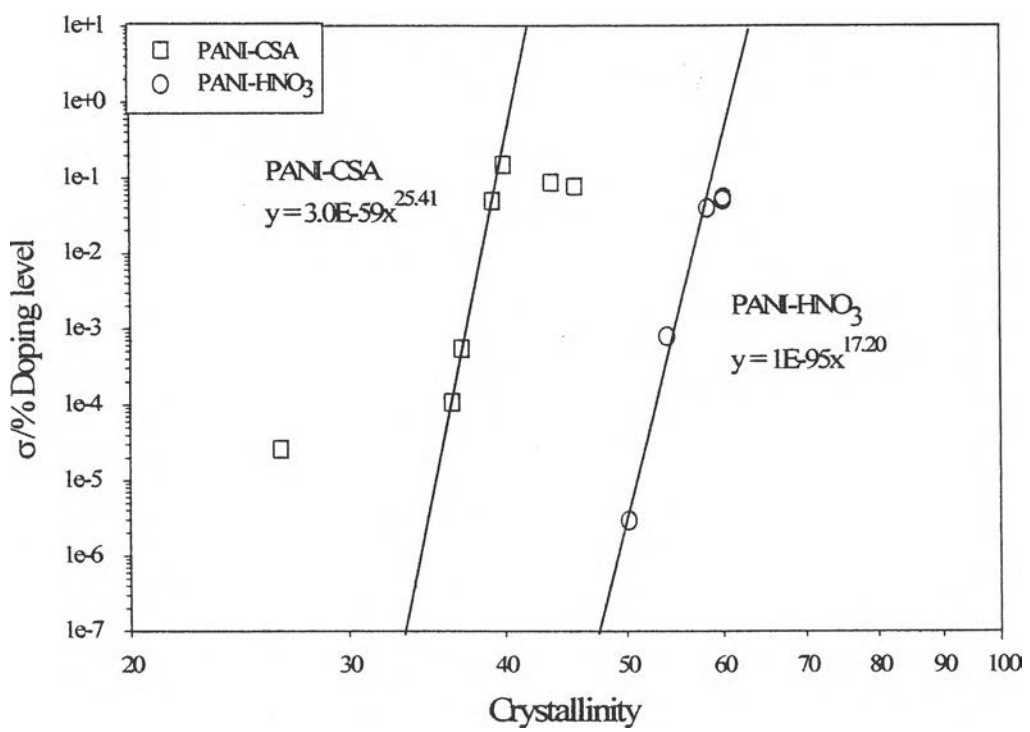

Figure 4.13 σ/doping level (%) vs. the crystallinity of PANI-CSA and PANI-HNO_3 (N_A/N_{EB} = 0.2, 0.5, 1.0, 2.0, 5.0, 10.0 and 20.0).

From equation $\sigma = ne\mu$; the carrier mobility is proportional to σ/% doping level. From Figure 4.13, a power law relation between σ/% doping level and a[%crystallinity]^b was found for both PANI-CSA and PANI-HNO_3. This implies that the carrier mobility is then proportional to [%crystallinity]^b. The equation of $y = 3.0E\text{-}59x^{25.41}$ was found for PANI-CSA and $y = 1.0E\text{-}95x^{17.20}$ was found for PANI-HNO_3. The slopes of the two lines are 25.41 and 17.20 for PANI-CSA and PANI-HNO_3, respectively. PANI-CSA has a higher slope value than that of PANI-HNO_3, implying that the charge mobility of PANI-CSA depended more strongly on % crystallinity than that of PANI-HNO_3. This may also imply that PANI-CSA possibly has a different macroscopic structure; they might have ordered regions of smaller sizes than those of PANI-HNO_3, as proposed in Figure 4.14.

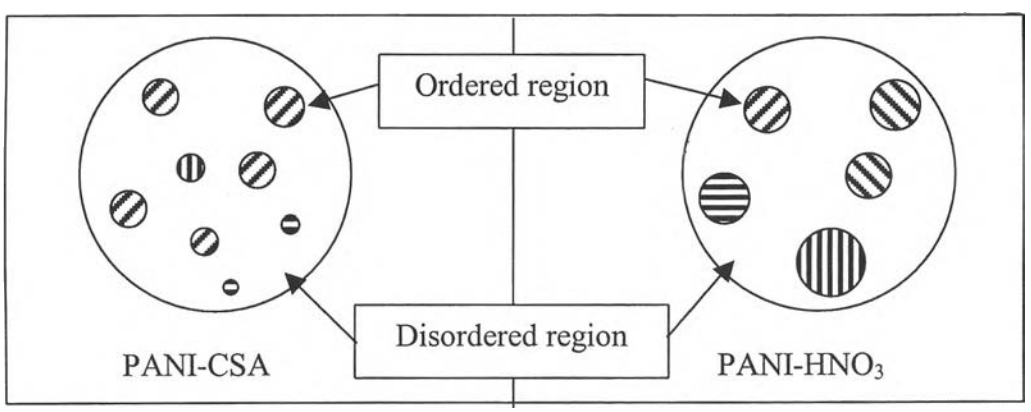

Figure 4.14 Proposed model for PANI-CSA and PANI-HNO_3 in terms of carrier mobility and the crystallinity.

From Figure 4.14, PANI-CSA is proposed to have ordered regions of smaller sizes than those of PANI-HNO_3. PANI-CSA possessed higher specific conductivity at the same value of % crystallinity. Ordered regions of smaller sizes led to a better electron movement through the PANI-CSA structure.

4.2.3 Effect of Amount of Polyimide in the Blend

The specific conductivity values of PANI-CSA and PANI-HNO_3 (N_A/N_{EB} = 10) blended with polyimide at various blend ratios (1, 5, 10, 20, 30, 50, 70, 75 and 80 % w/w), at a controlled temperature between 25 ± 2 °C, a relative humidity in air between 48-52 % and at the atmospheric pressure 1 atm were measured in order to study on the effect of %wt of polyimide in the blend on the specific conductivity. The effect of blend ratio on the specific conductivity of doped polyaniline is shown in Figure 4.15.

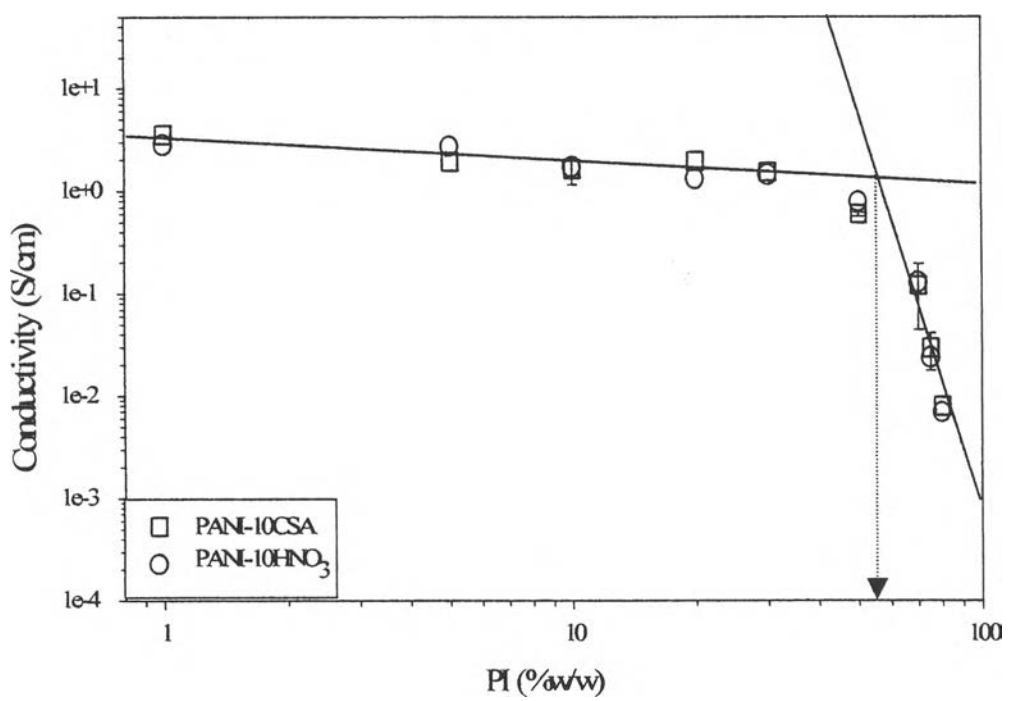

Figure 4.15 Conductivity vs. PI (%w/w) of PANI-CSA and PANI-HNO_3 (N_A/N_{EB} = 10, %wt of PI = 1, 5, 10, 20, 30, 50, 70, 75 and 80).

From Figure 4.15, the plot between the specific conductivity and the %wt polyimide shows a percolation threshold around 45 %wt for both PANI-CSA and PANI-HNO_3. This percolation threshold value is quite high when compared with

that previous work (5%, Cao *et. al*, 1992) employing the dry mixing between polyaniline with polyimide. Also, the result from TGA in part 4.1.3.2 confirms no interaction between polyaniline and polyimide. In 2000, Valenciano *et al.* reported a low value of percolation threshold at 5 %wt of polyaniline but they obtained relatively a low value of the specific conductivity at 10^{-2} S/cm. This was because of their solvent mixing method, which might have induced some changes in the morphology of polyaniline structures. In our work, the specific conductivity at percolation point could be as high as 0.32 and 0.26 S/cm for PANI-CSA and PANI-HNO_3, respectively.

4.3 Conductivity Response and Interaction to CO

A four point probe meter in the gas analyzing unit was used to measure the specific conductivity upon exposure to CO gas at various concentrations by a serial dilution method. The ambient pressure was 1 atm., and the open-air humidity was 48-52%. The conductivity of doped polyanilines and doped polyaniline blends with polyimide upon exposure to CO was increased with increasing CO gas concentration. Figure 4.16 shows the electrical conductivity response upon exposure to CO at 1000 ppm for PANI-10CSA.

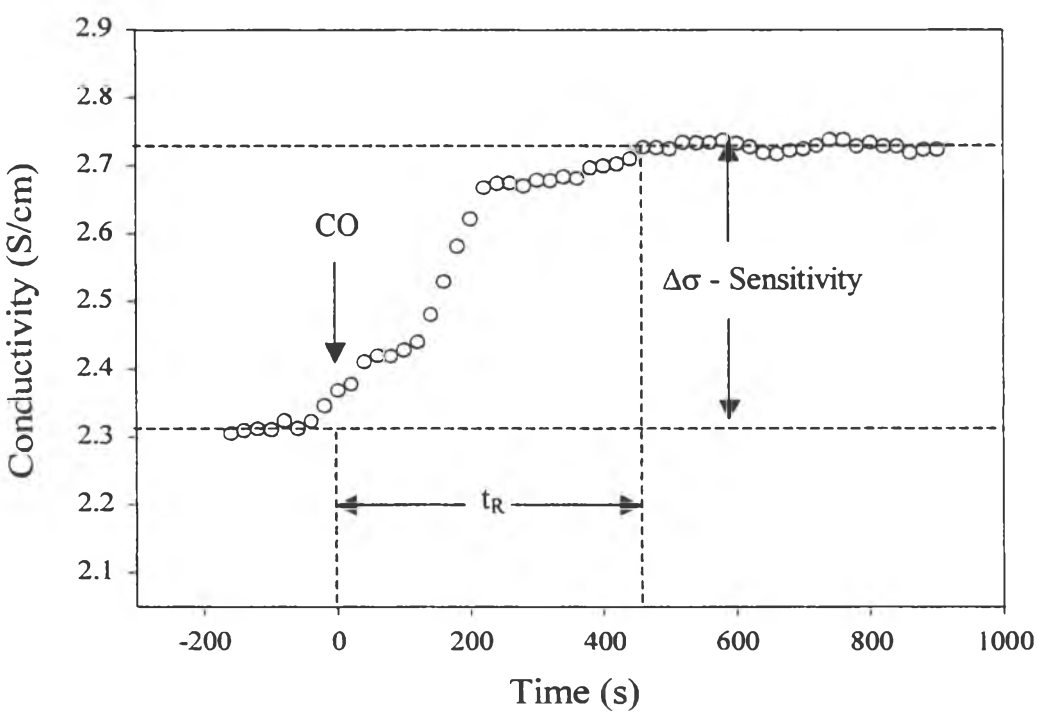

Figure 4.16 Electrical conductivity response upon exposure to CO at 1000 ppm of PANI-10CSA.

From Figure 4.16, the response of polyaniline upon exposure to CO at extensive time can be used to find the temporal response time (t_R) and the sensitivity

($\Delta\sigma$). The temporal response time is the duration between the time at the start of exposing until the time at which the conductivity reaches a saturated value (signal fluctuation < 10%). The sensitivity was calculated from the conductivity at saturation value subtracted by the conductivity of the exposure time equal to 0.

The mechanism of CO gas response of doped PANI is still not clear. The in-situ FT-IR spectrum upon exposed to CO at extensive of time was measured in an environmental cell where the specimens consisted of doped PANI as a KBr pellet (2-5 %wt). The peaks and assignments were found to be the same as those obtained without an exposure and consistent with those cited in the references of Appendix C, Table C.1. The in-situ FT-IR absorption peaks of PANI-CSA and PANI-HNO_3 upon exposed to CO is shown in Figure C.1 and Figure C.2, respectively.

However, one possibility of electrical conductivity response mechanism of doped polyaniline, p-type semiconducting material, upon exposing to CO, oxidixing gas, is proposed chemically in the Figure 4.17.

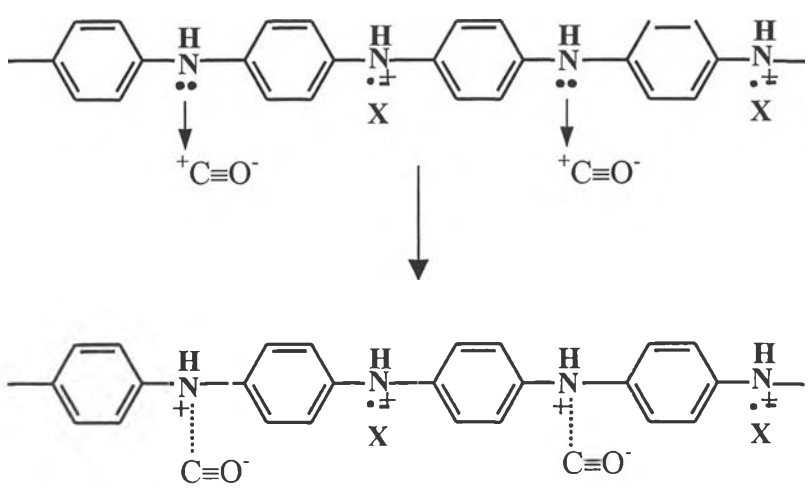

Figure 4.17 Gas response mechanism of doped polyaniline upon expose to CO.

Figure 4.17 is one of the possible mechanisms for doped PANI upon exposed to CO. It has a stable resonance as $^{+}C{\equiv}O^{-}$ then the positive charge at carbon

atom will withdraw a lone pair electron at amine nitrogen. The positive charges at carbon atom will then become neutral and amine nitrogen then possesses a positive charge. This results in the increase in the specific conductivity due to increase in the number of charge carrier; in our case, the positive charge is the charge carrier and the increment of conductivity is related to the amount of CO.

4.3.1 Doped Polyaniline

4.3.1.1 Effect of dopant type on conductivity response to CO

The conductivity response upon exposure to CO of PANI-1CSA and PANI-1HNO_3, at a controlled temperature between 25 ± 2 °C, a relative humidity in air between 48-52 % and at the atmospheric pressure 1 atm were recorded in order to study the effect of dopant type on sensing property to CO at the concentration 1000, 500, 250, 125, 62.5, 31.25, 15.63 and 7.81 ppm. Figure 4.18 shows the conductivity response to CO of PANI-1CSA and PANI-1HNO_3.

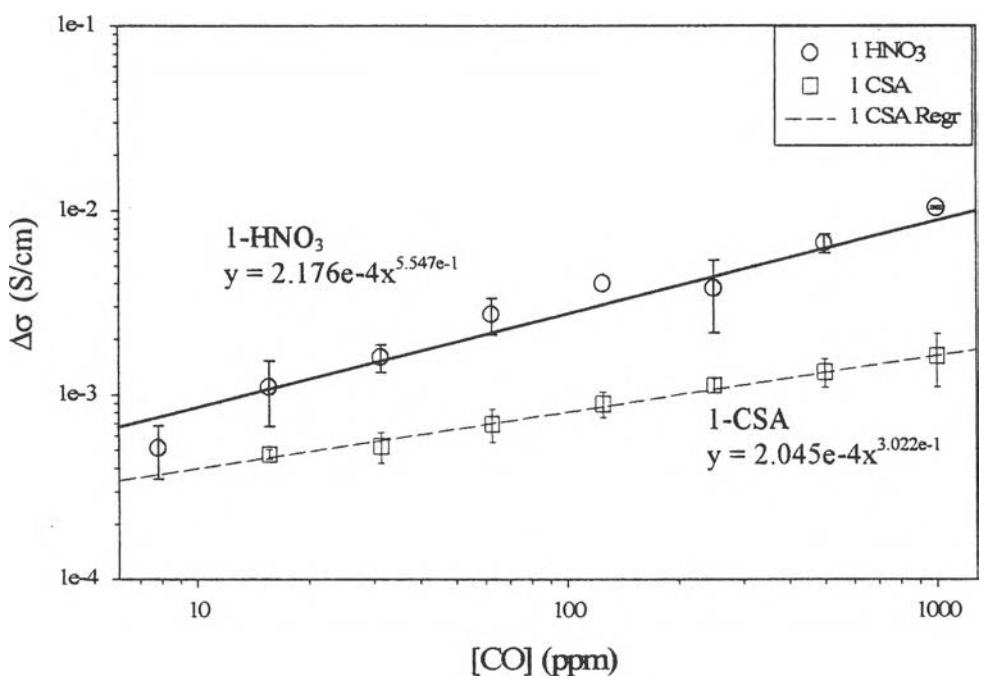

Figure 4.18 $\Delta\sigma$ vs. [CO] of PANI-CSA and PANI-HNO_3 at N_A/N_{EB} = 1.

From Figure 4.18, the electrical conductivity responses to CO of PANI-CSA and PANI-HNO_3 at N_A/N_{EB} = 1 at various CO concentrations are fitted to the equation of power law relation: $\Delta\sigma = a[CO]^b$, where 'a' is the intercept, 'b' is the slope of the graph when plot between log-log in both x and y-axis. The value of 'a' characterizes the intercept. The slope of the curve, b, can be used to characterize the concentration dependence which is proportional to the $d\Delta\sigma/dc$.

Consider the equation of $y = 2.176e\text{-}4x^{5.547e\text{-}1}$ for PANI-HNO_3 and $y = 2.045e\text{-}4x^{3.022e\text{-}1}$ for PANI-CSA. Consider the value of 'b' which is related to the concentration dependence. PANI-HNO_3 has a higher concentration dependence value due to the more ordered structure of PANI-HNO_3 according to the % crystallinity. From XRD data, the % crystallinity of PANI-HNO_3 is 60.04 % while that of PANI-CSA is 45.47 %. In 1991, Pouget *et al.* proposed the ordered-disordered region or the metallic island model. In their works, they concluded that in the ordered region electrons has higher effective movement than partially ordered and disordered region. These are due to easier movement of electrons along the chain, interchain hoping and end-to-end jumping. This implies that the more ordered structure leads to an easier movement of electron. This occurred because of the effects of Δn and $\Delta\mu$, that can be obtained from $\sigma = ne\mu$ as $\Delta\sigma = e(\Delta n\mu + n\Delta\mu)$. The first term ($\Delta n$) comes from the change in amount of attack sites and accessibility. The second term ($\Delta\mu$) comes from the change in the carrier mobility. The value of Δn of both PANI-CSA and PANI-HNO_3 is comparable, when same amount of gas is exposed. So the significantly higher value of μ of PANI-HNO_3 than PANI-CSA led to the greater change in $\Delta\sigma$. This is the reason why and PANI-HNO_3 has greater concentration dependence than PANI-CSA. Up to now, there is no supporting evidence that the change in carrier mobility has led to the change in $\Delta\sigma$.

4.3.1.2 Effect of dopant concentration on conductivity response to CO

The conductivity responses upon exposed to CO of PANI-1CSA at N_A/N_{EB} = 1 and 10, at a controlled temperature between 25 ± 2 °C, a relative humidity in air between 48-52 % and at the atmospheric pressure 1 atm were recorded in order to study the effect of dopant concentration on sensing property to

CO at the concentration 1000, 500, 250, 125, 62.5, 31.25, 15.63 and 7.81 ppm. Figure 4.19 shows the conductivity response to CO of PANI-CSA at N_A/N_{EB} = 1 and 10.

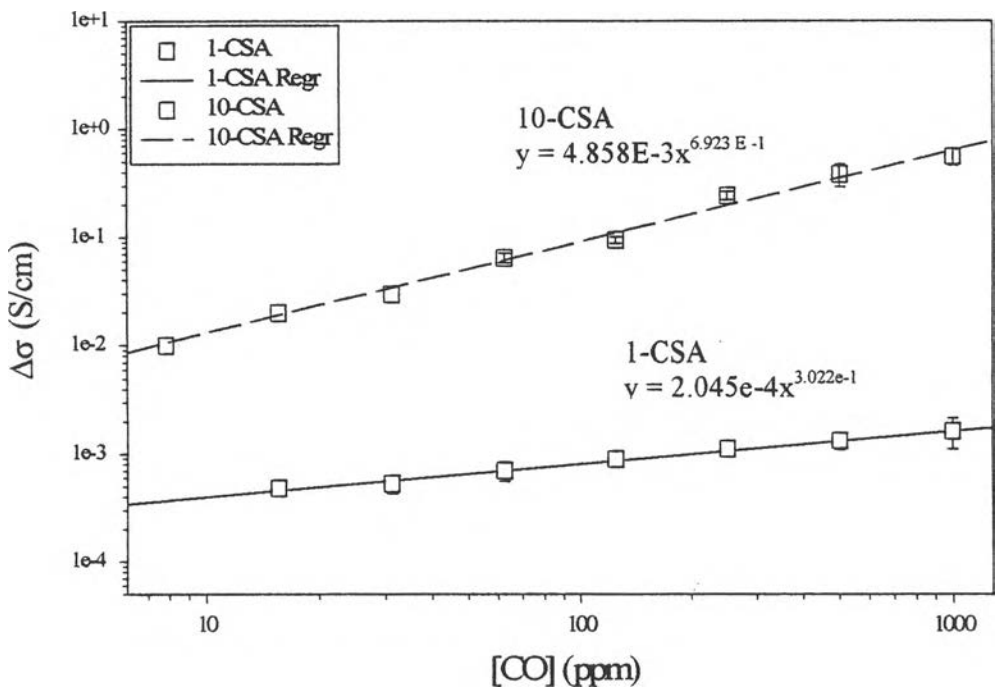

Figure 4.19 $\Delta\sigma$ vs. [CO] of PANI-CSA at N_A/N_{EB} = 1 and 10.

From Figure 4.19, the electrical conductivity responses to CO of PANI-CSA at N_A/N_{EB} = 1 and 10, at various CO concentrations are fitted to the equation of power law relation: $\Delta\sigma = a[CO]^b$, where a is the intercept, b is the slope of the graph when plot between log-log in both x and y-axis.

Consider the equation of $y = 4.858e\text{-}3x^{6.923e-1}$ for N_A/N_{EB} = 10 and $y = 2.045e\text{-}4x^{3.022e-1}$ for N_A/N_{EB} = 1. The 'a' value of doping ratio N_A/N_{EB} = 10 is higher than those of doping ratio N_A/N_{EB} = 1, due to the more ordered structured from % crystallinity of doping ratio 10. This can be explained in terms of trapping model that gas could hardly attack amine nitrogen because of the higher density structure and at the same time it could hardly be taken out also. So the 'a' value of N_A/N_{EB} =

10 is greater than that of N_A/N_{EB} = 1. As for the 'b' value, polyaniline at a doping ratio 10 (0.69) has a higher concentration dependence value compared with polyaniline at doping ratio 1 (0.30). This occurred because of the effects of Δn and $\Delta\mu$, that can be obtained from $\sigma = ne\mu$ as $\Delta\sigma = e(\Delta n\mu + n\Delta\mu)$. The first term ($\Delta n$) comes from the change in amount of attack sites and accessibility. The second term ($\Delta\mu$) comes from the change in the carrier mobility. PANI-CSA at doping ratio 10 had a better accessibility along with higher values % crystallinity generating more ordered structures. This led to the higher product, $\Delta\sigma$, that lead to the higher value of 'b' than that of PANI-1CSA.

4.3.1.3 Effect of temperature on conductivity response to CO

The conductivity responses upon exposure to CO of PANI-CSA and PANI-HNO_3 at N_A/N_{EB} = 10, at a controlled temperature between 25 ± 2, 35 ± 2, 45 ± 2 and 55 ± 2 °C, a relative humidity in air between 48-52 % and at the atmospheric pressure 1 atm were recorded in order to study the effect of temperature on sensing property to CO at the concentration 1000, 500, 250, 125, 62.5, 31.25, 15.63 and 7.81 ppm. The correlation between the sensing property and CO at various temperatures are summarized in the Tables 4.1 and 4.2 for PANI-CSA and PANI-HNO_3, respectively; whereas the relationship $\Delta\sigma = a[CO]^b$ are found for all sample sets.

Table 4.1 Concentration dependence value (b) and the intercept (a) from the plot between $\Delta\sigma$ and [CO] (ppm) for PANI-CSA (N_A/N_{EB} = 10) at 25 ± 2, 35 ± 2, 45 ± 2 and 55 ± 2 °C

Temperature (°C)	a	b
25	4.86E-03	0.69
35	6.31E-02	0.44
45	4.85E-02	0.37
55	2.07E-02	0.17

Table 4.2 Concentration dependence value (b) and the intercept (a) from the plot between $\Delta\sigma$ and [CO] (ppm) for PANI-HNO_3 (N_A/N_{EB} = 10) at 25 ± 2, 35 ± 2, 45 ± 2 and 55 ± 2 °C

Temperature (°C)	a	b
25	1.79E-03	0.83
35	2.92E-02	0.46
45	1.28E-01	0.26
55	7.76E-02	0.30

The concentration dependence values at various temperatures of both PANI-CSA and PANI-HNO_3 at N_A/N_{EB} = 10 were plotted in order to study the correlation between temperature and the concentration dependence value as shown in Figure 4.20.

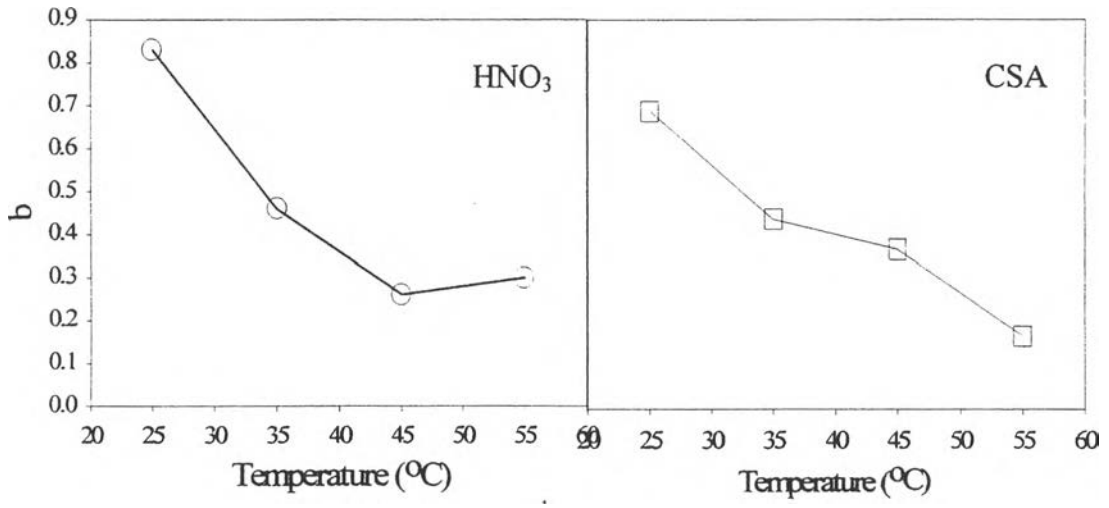

Figure 4.20 Concentration dependence vs. temperatures of PANI-CSA and PANI-HNO_3 at N_A/N_{EB} = 10.

From Figure 4.20, the concentration dependences decreases with increasing temperature for both PANI-CSA and PANI-HNO_3 at all temperatures. This was so because the kinetic energy of gas was greater at higher temperature leading to a faster movement. So the chance of gas to attack at the amine nitrogen was less, resulting in a smaller change in conductivity upon an exposure to the same amount of CO. An exception was at 55 °C for PANI-HNO_3; it had a higher value of 'b' than that at 45 °C. The reason for this was not clear. This might be related to the kinetic energy model as will be described in section 4.3.2.

4.3.1.4 Effect of acid type and concentration on temporal response time

The conductivity response upon exposure to CO of PANI-CSA and PANI-HNO_3 at N_A/N_{EB} = 1, at a controlled temperature between 25 ± 2 °C, and at N_A/N_{EB} 10, at controlled temperature of 25 ± 2, 35 ± 2, 45 ± 2 and 55 ± 2 °C, a relative humidity in air between 48-52 % and at the atmospheric pressure 1 atm were recorded in order to study the effect of acid type and concentration on temporal response time upon exposure to CO at the concentration 1000 ppm. The temporal

response times are summarized in the Tables 4.3 and 4.4 for PANI-CSA and PANI-HNO_3, respectively. All data shown are averaged values taken from at least 2 data points.

Table 4.3 Temporal response times (minute) of PANI-CSA (N_A/N_{EB} = 1 and 10) at 25 ± 2, 35 ± 2, 45 ± 2 and 55 ± 2 °C at [CO] = 1000 ppm

Temperature (°C)	N_A/N_{EB} = 1	N_A/N_{EB} = 10
25	31.0	22.1
35	N/A	56.4
45	N/A	80.3
55	N/A	47.2

Table 4.4 Temporal response times (minute) of PANI-HNO_3 (N_A/N_{EB} = 1 and 10) at 25 ± 2, 35 ± 2, 45 ± 2 and 55 ± 2 °C at [CO] = 1000 ppm

Temperature (°C)	N_A/N_{EB} = 1	N_A/N_{EB} = 10
25	36.8	18.6
35	N/A	68.8
45	N/A	59.3
55	N/A	67.2

From Tables 4.3 and 4.4, the effect of acid types on temporal response time is uncertain. The data are not sufficient to conclude which one offers a faster signal upon exposed to CO. In terms of acid concentration, we found that the temporal response time of lower doping ratio N_A/N_{EB} = 1 was higher than that of doping ratio

N_A/N_{EB} = 10. This can be explained in term of the density of the structure; the higher doping ratio led to the more % crystallinity as concluded in section 4.2.2. So the possibility for CO to react with the attack site and became saturated for N_A/N_{EB} = 10 was more likely than that of N_A/N_{EB} = 1.

For the effect of temperature on the temporal response time, the temporal response time increased with increasing temperature. This was due to the higher kinetic energy of gas as described in section 4.3.1.3; CO molecules were more excited at higher temperature. It had a lesser chance to react with polyaniline and took more time to reach the saturated value.

4.3.2 Doped Polyaniline Composite with Polyimide

4.3.2.1 Effect of temperature on the conductivity response to CO of the composite

The conductivity responses upon exposure to CO of PANI-CSA and PANI-HNO_3 at N_A/N_{EB} = 10 composite with 30 %wt polyimide, at controlled temperatures of 25 ± 2, 35 ± 2, 45 ± 2 and 55 ± 2 °C, a relative humidity in air between 48-52 % and at the atmospheric pressure 1 atm were recorded in order to study the effect of temperature on conductivity response to CO at the concentration 1000, 500, 250, 125, 62.5, 31.25, 15.63 and 7.81 ppm of polyaniline/polyimide composite.

The reason of choosing the composite at 30 %wt of polyimide in polyaniline matrix wass because of the specific conductivity of the composite was sufficiently high ($\sigma \sim 1.14$ and 0.64 S/cm for PANI-CSA and PANI-HNO_3, respectively) and because of our instrumental limitations ($I \sim 40$ mA, $V_{app} \sim 30$ V and $V_d \sim 9.99$ V). In addition, the highest content of polyimide was expected for improved thermal stability..

The correlations between the conductivity response to CO at various temperatures of PANI-CSA and PANI-HNO_3 at N_A/N_{EB} = 10 and the composites containing PANI-CSA and PANI-HNO_3 at N_A/N_{EB} = 10 with 30 %wt polyimide were plotted together and shown in Figures 4.21 – 4.24 for PANI-CSA and Figures 4.25 – 4.28 for PANI-HNO_3, respectively.

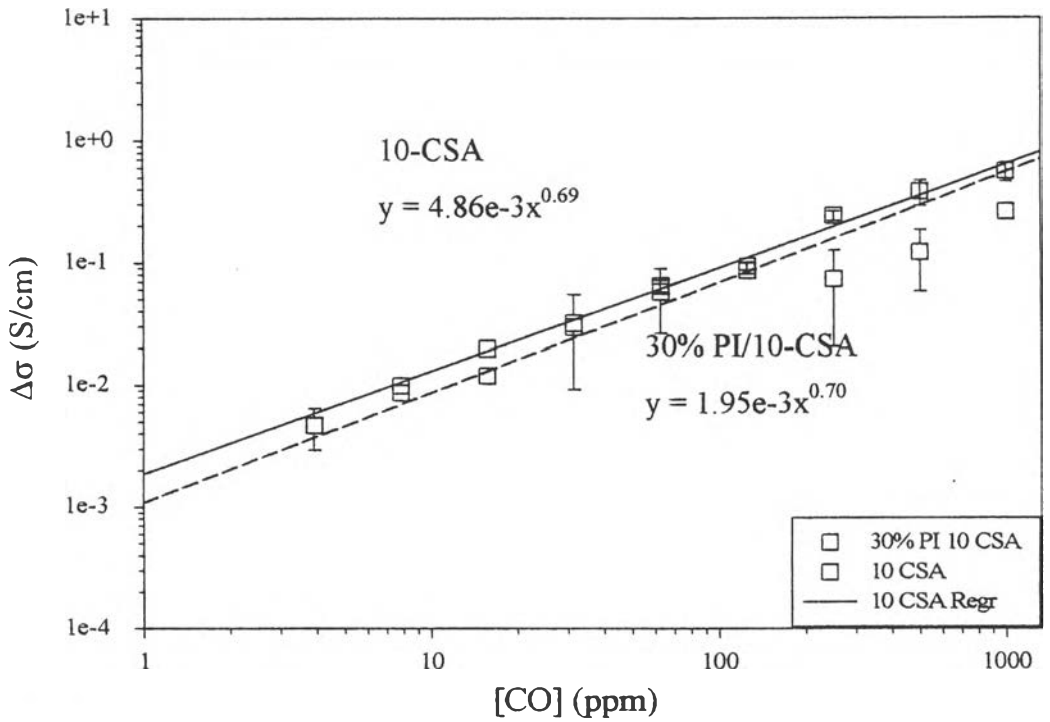

Figure 4.21 Δσ vs. [CO] of PANI-10CSA and PANI-10CSA/30 %wt PI at 25 °C.

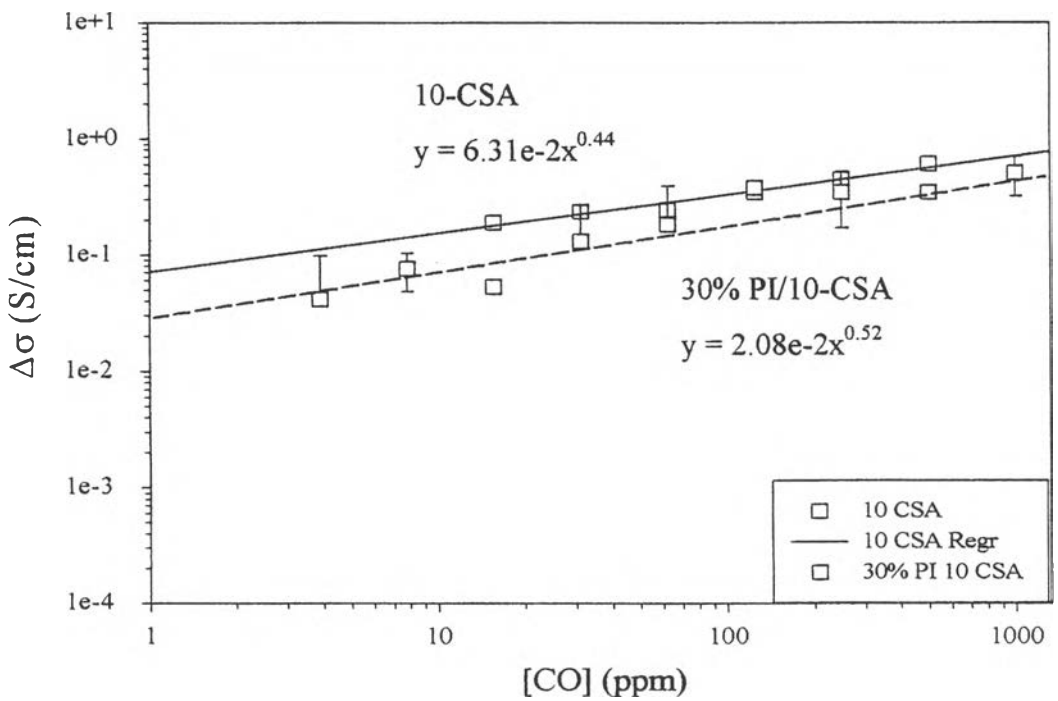

Figure 4.22 Δσ vs. [CO] of PANI-10CSA and PANI-10CSA/30 %wt PI at 35 °C.

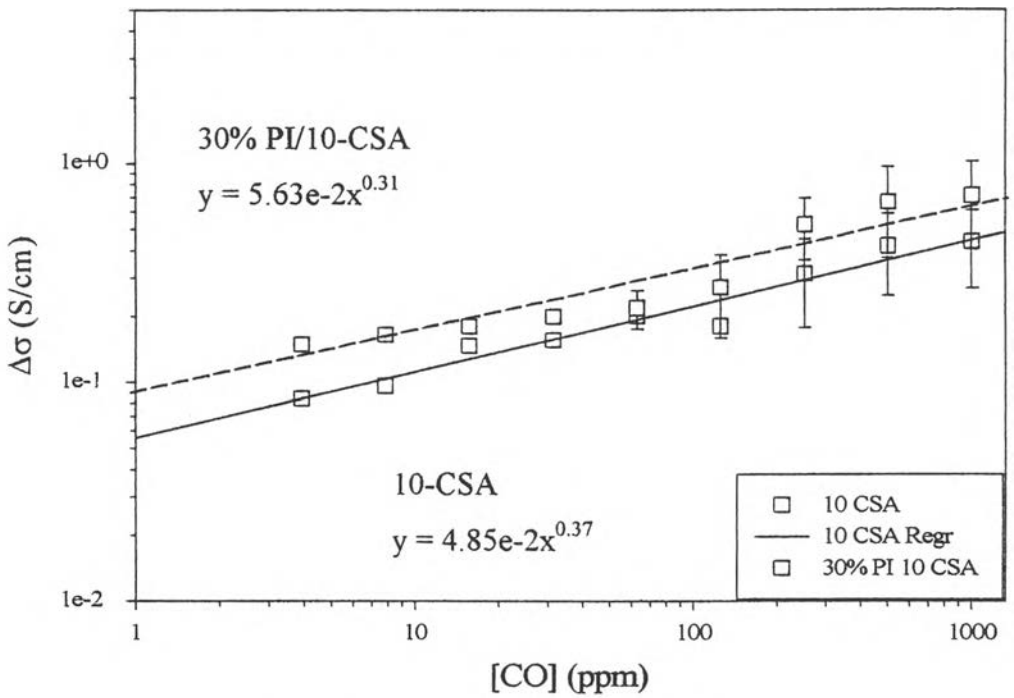

Figure 4.23 Δσ vs. [CO] of PANI-10CSA and PANI-10CSA/30 %wt PI at 45 °C.

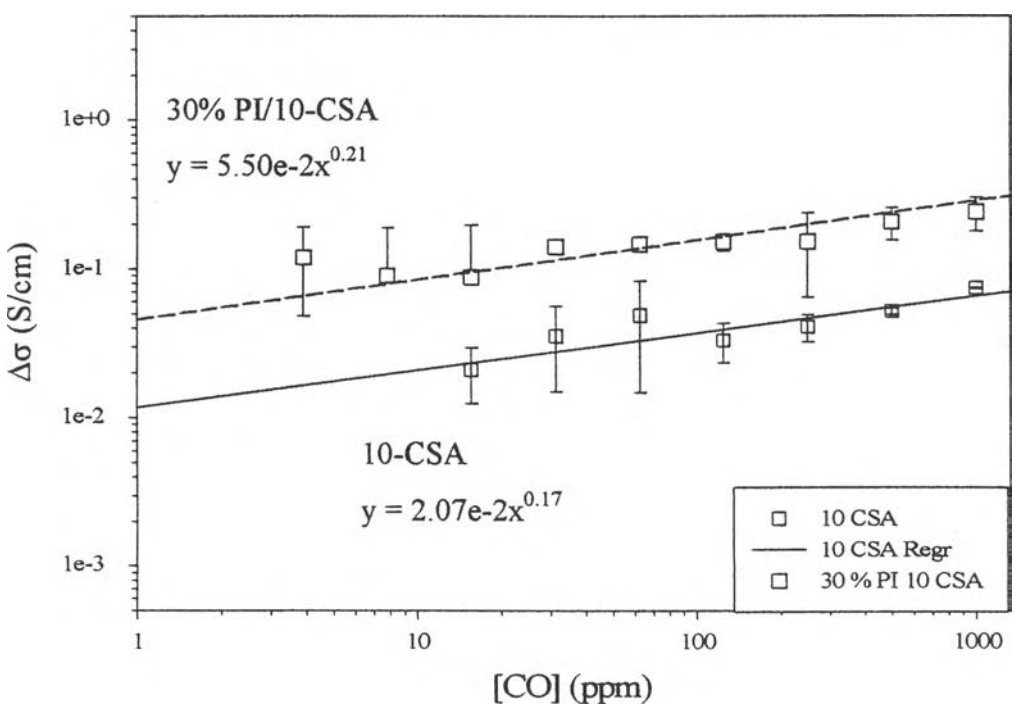

Figure 4.24 Δσ vs. [CO] of PANI-10CSA and PANI-10CSA/30 %wt PI at 55 °C.

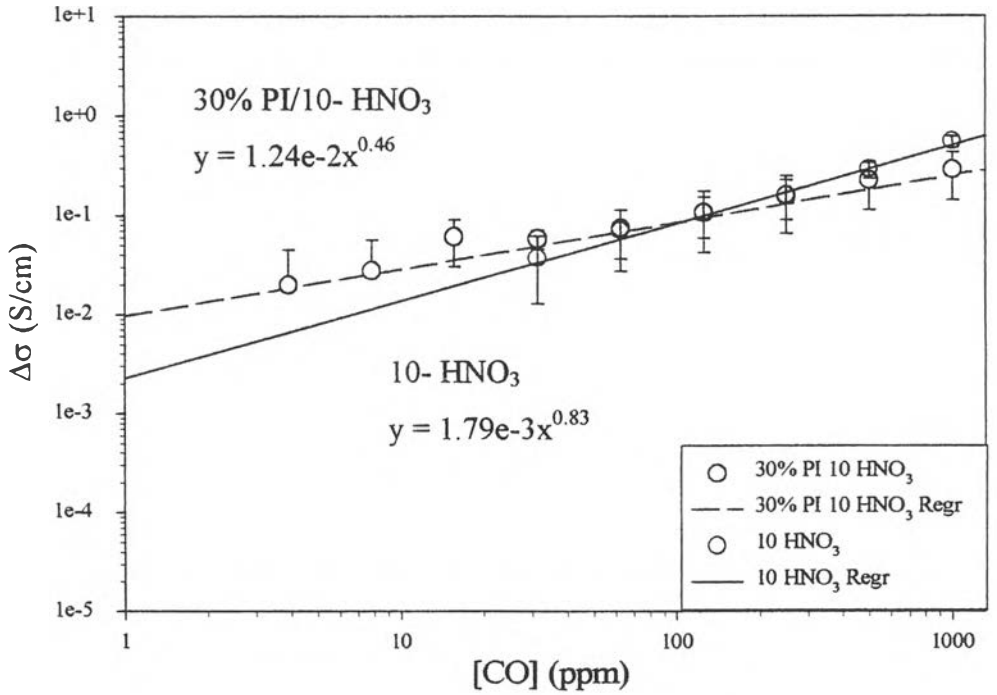

Figure 4.25 Δσ vs. [CO] of PANI-10HNO_3 and PANI-10HNO_3/30% PI at 25 °C.

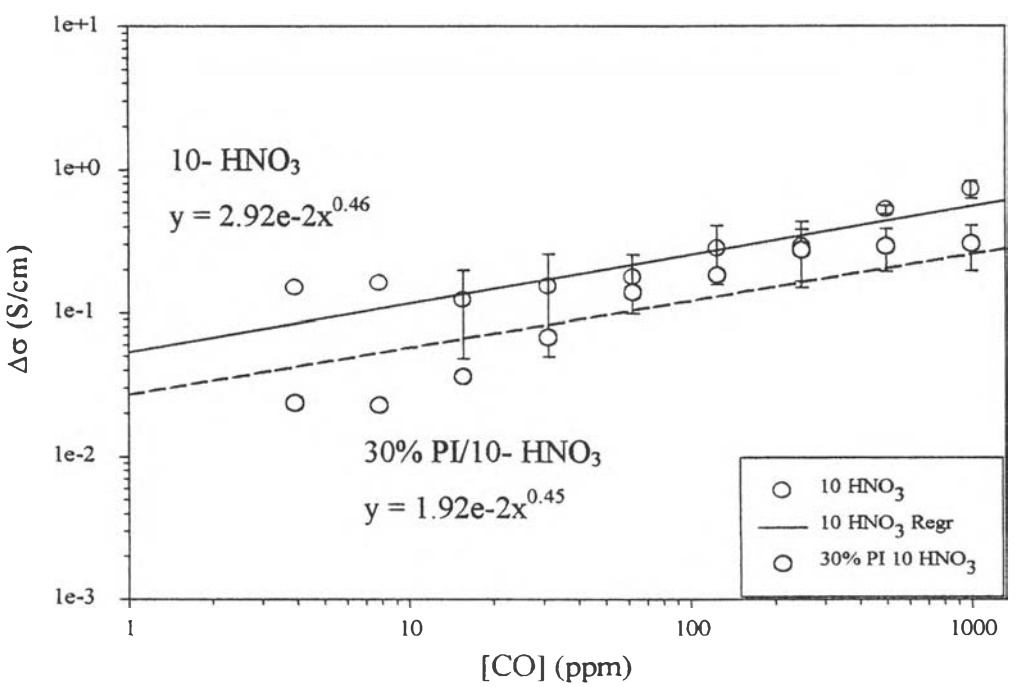

Figure 4.26 Δσ vs. [CO] of PANI-10HNO_3 and PANI-10HNO_3/30% PI at 35 °C.

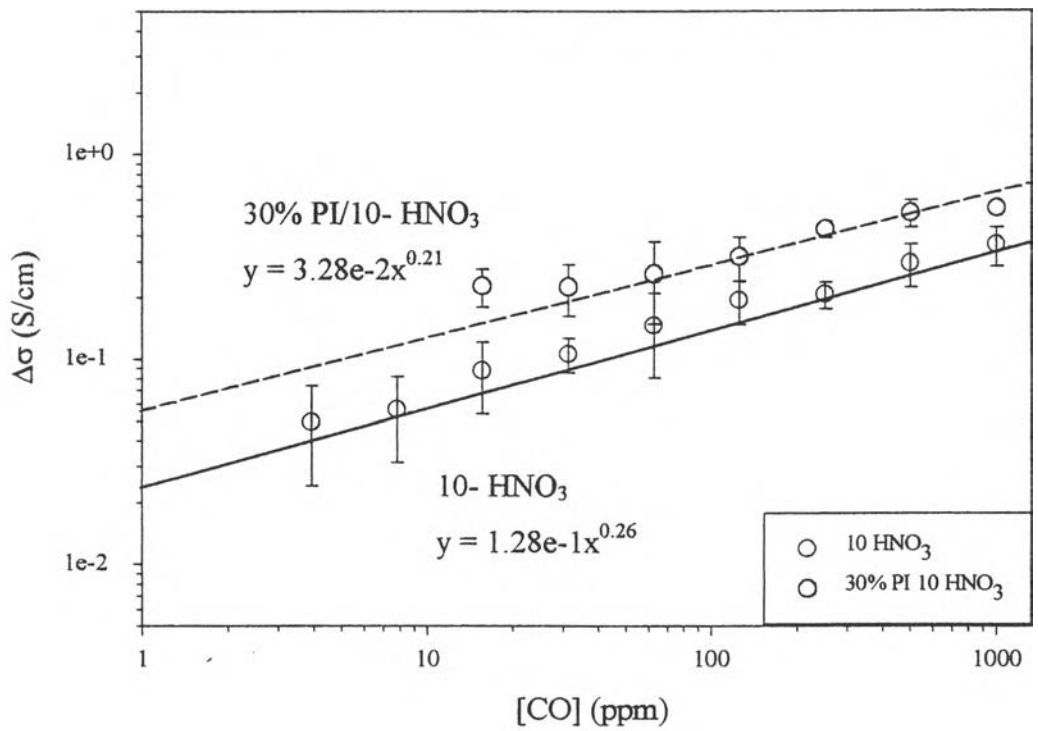

Figure 4.27 $\Delta\sigma$ vs. [CO] of PANI-10HNO_3 and PANI-10HNO_3/30% PI at 45 °C.

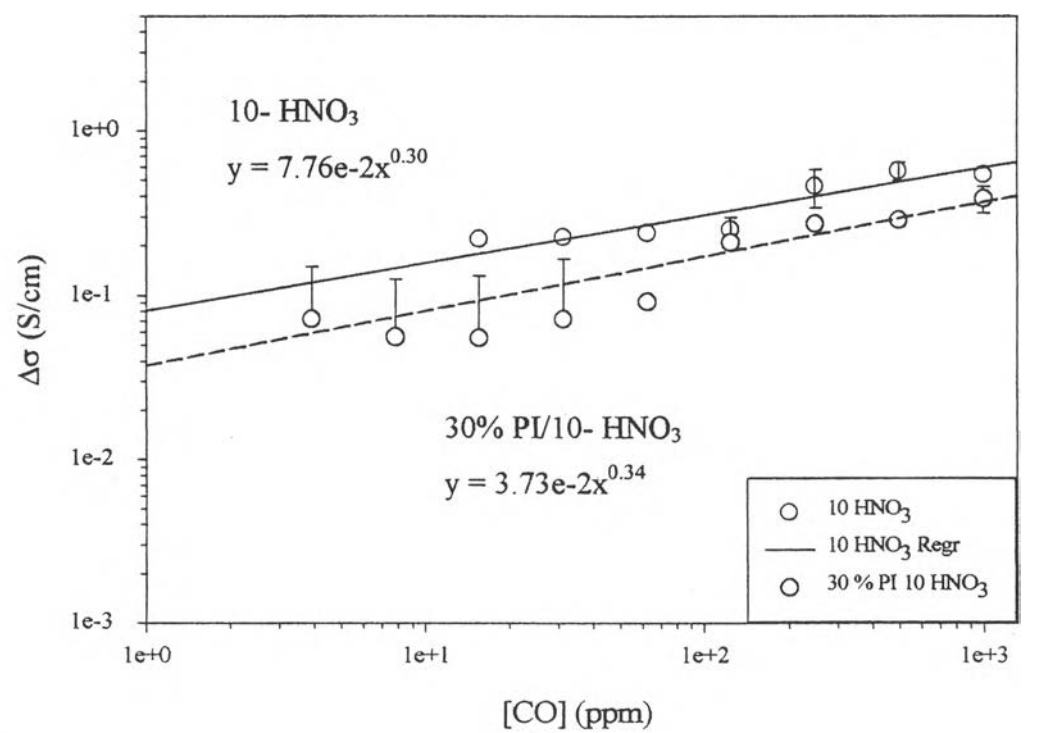

Figure 4.28 $\Delta\sigma$ vs. [CO] of PANI-10HNO_3 and PANI-10HNO_3/30% PI at 55 °C.

The values of a-intercept and b-slope of the relation $\Delta\sigma = a[CO]^b$, for PANI-CSA and PANI-HNO_3 at N_A/N_{EB} = 10 and the composites containing PANI-CSA and PANI-HNO_3 at N_A/N_{EB} = 10 with 30 %wt polyimide, are summarized in the Tables 4.5 and 4.6.

Table 4.5 Values of a-intercept of the curve $\Delta\sigma = a[CO]^b$ of pure and blend at various temperatures

Temperature (°C)	PANI-10CSA		PANI-10HNO_3	
	pure	30 %wt PI	Pure	30 %wt PI
25	4.86E-03	1.95E-03	1.79E-03	1.24E-02
35	6.31E-02	2.08E-02	2.92E-02	1.92E-02
45	4.85E-02	5.63E-02	1.28E-01	3.28E-02
55	2.07E-02	5.50E-02	7.76E-02	3.73E-02

Table 4.6 Values of b-slope of the curve $\Delta\sigma = a[CO]^b$ of pure and blend at various temperatures

Temperature (°C)	PANI-10CSA		PANI-10HNO_3	
	pure	30 %wt PI	Pure	30 %wt PI
25	0.69	0.70	0.83	0.46
35	0.44	0.52	0.46	0.45
45	0.37	0.31	0.26	0.21
55	0.17	0.21	0.30	0.34

From Table 4.6, the value of 'b' decreases with increasing temperature for both pure and 30 %wt PI and for both PANI-CSA and PANI-HNO_3. The decreases are due to the kinetic energy of gases as discussed in detail in section 4.3.1.3. There was no significant difference in the value of 'b' at higher temperatures for pure and

composites made of PANI-CSA. It can be concluded that the concentration dependence is a function of temperature. The deviation in the value of 'b' can be explained in terms of the larger particle size of PANI-10CSA (particle size = 29 μm) as compared to that of PANI-10HNO_3 (particle size = 17 μm) doped polyaniline and polyimide (particle size = 32 μm) as shown in Figure 4.29.

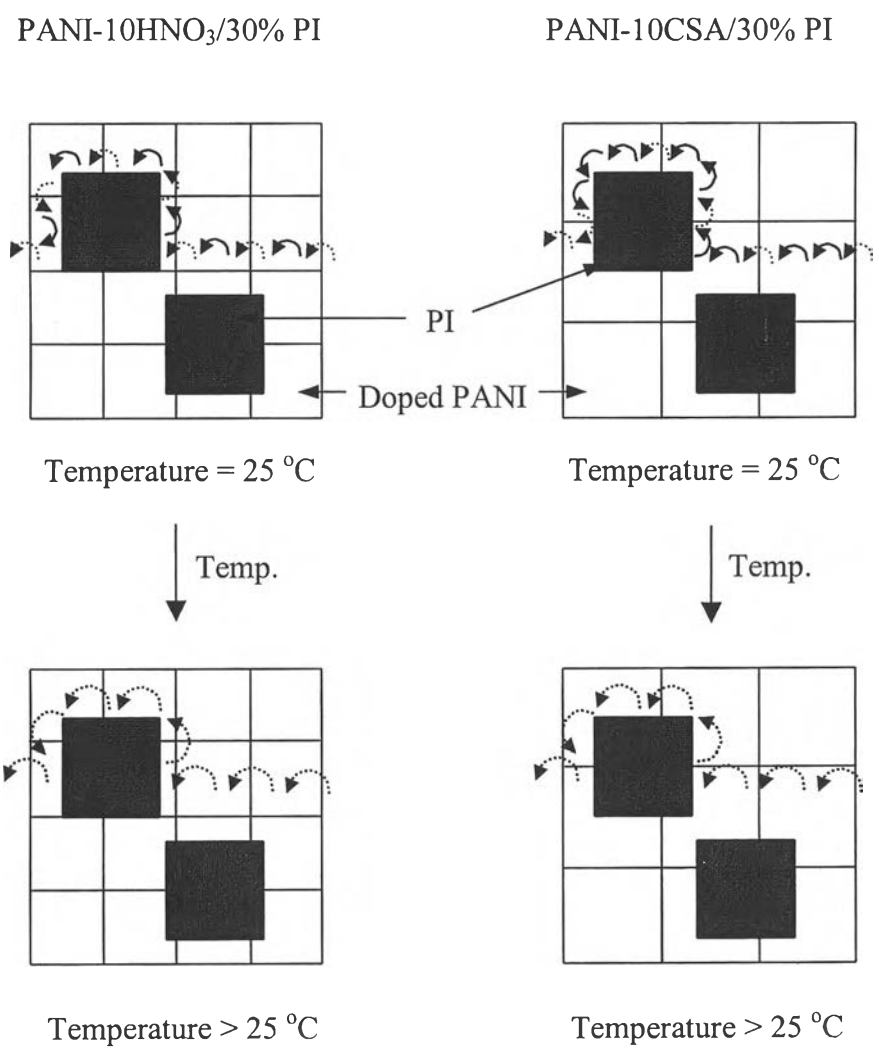

Figure 4.29 Proposed model for electron movement of PANI-10CSA/30% PI and PANI-10HNO_3/30% PI at room temperature and at a higher temperature.

From Figure 4.29, each open square represents one particle of PANI-HNO_3 and PANI-CSA and each dark square represents one particle of PI. The dotted line arrow represents the movement of an electron from one particle to another particle and the solid line arrow represents a movement of electron within one particle. The movement of electron from one particle to another particle is more difficult than the movement of electron within one particle. At room temperature, PANI-10CSA/30% PI has a greater electronic movement throughout the structure. This was due to the larger particle size of PANI-10CSA than that of PANI-10HNO_3. At higher temperature, electron is more excited, so it can move more easily than at room temperature. So the value of 'b' of the composite is comparable to the pure at higher temperature for both PANI-HNO_3 and PANI-CSA.

4.3.2.2 Temporal response time of the composite

The conductivity responses upon exposure to CO of PANI-CSA and PANI-HNO_3 at N_A/N_{EB} = 10 blended with 30 %wt polyimide, at controlled temperatures of 25 ± 2, 35 ± 2, 45 ± 2 and 55 ± 2 °C, a relative humidity in air between 48-52 % and at the atmospheric pressure 1 atm were recorded in order to study the temporal response time upon exposure to CO at the concentration 1000 ppm. The temporal response times are summarized in the Tables 4.7 and 4.8 for pure or PANI-CSA/30% PI and PANI-HNO_3/30% PI doped polyanilines, respectively. All data were averaged from at least 2 data points.

Table 4.7 Temporal response time (minute) of PANI-CSA (N_A/N_{EB} = 10) pure and blend with 30 %wt polyimide at 25 ± 2, 35 ± 2, 45 ± 2 and 55 ± 2 °C at [CO] = 1000 ppm

Temperature (°C)	$t_{(pure)}$ (min)	$t_{(composite)}$ (min)
25	22.1	79.7
35	56.4	62.8
45	80.3	59.9
55	47.2	48.4

Table 4.8 Temporal response time (minute) of PANI-HNO_3 (N_A/N_{EB} = 10) pure and blend with 30 %wt polyimide at 25 ± 2, 35 ± 2, 45 ± 2 and 55 ± 2 °C at [CO] = 1000 ppm

Temperature (°C)	$t_{(pure)}$ (min)	$t_{(composite)}$ (min)
25	18.6	55.5
35	68.8	66.4
45	59.3	60.7
55	67.2	55.0

From Table 4.7, the temporal response times of PANI-CSA (N_A/N_{EB} = 10) pure (22.1 minute) and blend with 30 %wt polyimide (79.7 minute) at room temperature are quite different. This was due to the barrier effect of polyimide through the doped polyaniline structure. As the number of gas response sites was decreased in the composite containing 30 %wt polyimide relative to that of the pure polyaniline, the time it took to reach the equilibrium was longer. The same result for PANI-HNO_3 was obtained; they were 18.6 minute for pure and 55.5 minute for the

composite. At a higher temperature, the temporal response times were higher for both pure and composite and for both PANI-CSA and PANI-HNO_3. This may be due to the higher kinetic energy of gas as described in detail in section 4.3.1.4 that as the temperature increases, CO would move faster. Then the possibility of CO to incorporate into polyaniline chain was reduced.